Accepted for publication in Tribology Letters
Published in December, 2016
DOI: 10.1007/s11249-016-0798-0

Global approach of tribo-mechanical development of hybrid aluminum matrix syntactic foams

Kornél MÁJLINGER[a,1,*], Gábor KALÁCSKA[b,2], Imre Norbert ORBUULOV[a,c,3], László ZSIDAI[b,4], Benjámin BOZÓKI[a,5], Róbert KERESZTES[b,6]

[a]Budapest University of Technology and Economics, Faculty of Mechanical Engineering, Department of Materials Science and Engineering, H-1111 Bertalan Lajos str. 7. MT building, Budapest, Hungary

[b]Szent István University, Faculty of Mechanical Engineering, Institute for Mechanical Engineering Technology, H-2103, Páter Károly u. 1., Gödöllő, Hungary

[c]MTA–BME Research Group for Composite Science and Technology, H-1111 Műegyetem rakpart 3., Budapest, Hungary

[1]vmkornel@eik.bme.hu, [2]kalacska.gabor@gek.szie.hu, [3]orbulov@eik.bme.hu, [4]zsidai.laszlo@gek.szie.hu, [5]tucsokraj09@gmail.com, [6]keresztes.robert@gek.szie.hu,

[*]Corresponding author

Abstract

Hybrid syntactic foams with AlSi12 aluminum matrix were produced by pressure infiltration. The volume ratio of iron and ceramic hollow sphere reinforcement (in the same size range) was varied and hybrid syntactic foams were also produced with bimodal size ceramic reinforcement.

Previously a very detailed analysis of the mechanical properties of the composites was made with quasi-static compression tests and their tribological properties were investigated by pin-on-disc method in dry and lubricated conditions.
The present article establishes and clarifies the correlations between mechanical and tribological properties. The coefficient of friction, height loss of the specimens and specific wear showed good correlation to different mechanical parameters e.g. density, structural stiffness and yield strength.
The established trends and correlations between mechanical and tribological behavior enables a better understanding for materials design and selection for further applications for mechanically loaded sliding machine parts.

Keywords

Metal-matrix composite; Aluminum matrix syntactic foam; Hybrid composite; Pin-on-disc testing; Dry friction; Lubricated friction; Sliding wear

1. Introduction

Metal matrix syntactic foams (MMSFs) originates from their polymer matrix counterparts and they are consisting of a lightweight metallic matrix (usually some kind of aluminium alloy) and hollow spheres (normally ceramics, or metallic). These foams are often considered as composite metallic foams (CMFs) too. MMSFs have outstanding specific properties among the porous materials. Due to the hollow spheres, their specific compressive strength and energy absorbing capability are uniquely high [1].

The most common loading condition for MMSFs is compression (e.g. collision dampers, brake parts, anti-shock buffers, blast absorbing armors etc.), therefore their behaviour under compressive loading has been widely studied. For example, Gupta et al. [2-7] studied the quasi-static and high strain rate properties of various MMSF systems, such as Al-Al_2O_3 or more unique Al-SiC MMSFs. Rabiei et al. [8-10] developed CMFs with high energy absorbing capacity and revealed that the high strain rate and the quasi-static strain rate tests can overlap each other. Fiedler and Taherishargh et al. [11-15] produced low density and low cost syntactic foams, by the combination of Al alloys and expanded perlite. The authors proved the applicability of these set of foams by numerous versatile investigations. More recently hollow tubes were filled by their low density MMSFs [16]. The mechanical tests of the tubes revealed high energy absorption capacity and improved mechanical stability. Lehmhus and Weise et al. [17-20] and Castro et al. [21-22] investigated high strength, steel based syntactic foams under different conditions and found that although the density of the produced foams is higher, it is compensated by their higher strength and energy absorption. Goel et al. [23-25] focused on the effect of strain rate on the mechanical properties. Xue et al. [26, 27] successfully applied powder metallurgy to produce Ti based MMSFs that can be used in biomedical applications. All of the above mentioned researches confirm that MMSFs can be produced with various matrix materials and hollow spheres and their compressive properties can be tailored to the requirements of the desired structural parts. Besides the constituents, the microstructure (detailed in [28]) and the macrostructure [29] have decisive effect on the mechanical properties. For the investigation of the applicability of MMSFs for sliding machine parts (like bearings, pistons or cylinder bores), their tribological properties should be properly investigated, and furthermore it would be important to see the connections of mechanical properties to tribological behaviour as well. For a variety of aluminum matrix syntactic foams (AMSFs) reinforced with fly ash or cenosphere (ceramic hollow spheres) [30-38] dry wear characteristics and tribological properties were investigated with different methods some of them already in lubricated [30] conditions. The typical diameter of these reinforcements were less than 400 μm, and the density of the AMSFs bigger than 1.9 gcm^{-3}. Some tribological data is available for hybrid (hollow sphere + particle) reinforced AMSFs too [39], but only a few for hollow sphere + hollow sphere reinforced hybrid AMSFs [40, 41], with larger reinforcement size (Ø> 1mm). Also no literature was found in which correlations between mechanical and tribological properties of AMSFs were considered, however in tribology it is an essential knowledge in many aspects [42].

The main aim of our paper is to give data and broad support to (i) further development of such, porous materials in the aspect of tribological properties, (ii) the successful application of AMSFs (construction, expected lifetime etc.). As an additional feature the properties of the AMSFs and their trends are presented in the function of their reinforcing constituents (depending on the ratio of ceramic and metallic hollow spheres). To achieve this goal the measured tribological data of [41] and the mechanical properties of [48] were deeply analysed for correlations. The measured materials properties are detailed in the Materials and methods section in detail.

2. Materials and methods

2.1. Production of the AMSFs

As it was presented in details in [41] near eutectic AlSi12 alloy was chosen for the hybrid composites as matrix material, due to its good castability.

To produce the different AMSFs two grades of ceramic hollow spheres and one grade of metal hollow sphere reinforcement was used. The larger ceramic (commercial name: Globocer, GC) and the iron spheres (commercial name: Globomet, GM) were in the same size range (between Ø1.4-1.9 mm) and were provided by the same manufacturer, the Hollomet GmbH (Germany) [43], Germany. The smaller ceramic hollow spheres (commercial name: E-spheres, SLG) were produced by the Envirospheres Ltd. (Australia) [44]. The main properties of the matrix alloy and the hollow spheres are described in detail in [41].

To produce the AMSF blocks for further investigations low pressure infiltration was used. The infiltration pressure was 400 kPa, the temperature was 600°C and the infiltration time was 15 s. These pressure infiltration setup enables the highest reinforcement content which theoretical value for spheres (randomly close packed) is about 64 vol.% [45, 46]. More detailed description of the production method and the influence of the infiltration parameters are available in [28, 47, 48].

Two types of hybrid composites were produced with this infiltration technique. (I) The first hybrids were reinforced hollow spheres in the same size range, but with different reinforcement ratio, the GM and GC hollow sphere grades were mixed from 100 % GM – 0 % GC to 0 % GM – 100 % GC in 20 % steps of the achievable ~ 64 vol.% hollow sphere content. The specimens were designated after their reinforcement ratio: e.g. 80GM-20GC is a hybrid AMSF containing 80 vol.% GM and 20 vol.% GC grade hollow spheres (of the overall 64 vol.% reinforcement content). (II) An other type of hybrid AMSF was produced with bimodal reinforcement size from the ceramic SLG and GC grade reinforcements (almost identical composition, but one order of magnitude difference in the average diameter) and was designated as SLG+GC. In SLG+GC samples the calculated ratio of SLG reinforcement between the GC spheres was about 20 vol.%. AMSF with pure SLG reinforcement was also produced, for investigation of the size effect of the reinforcement.

Specimens for metallography, compressive tests and tribology tests were machined from the AMSF blocks, to avoid side effects [49], the specimen size for mechanical and tribological tests was Ø14 mm in diameter.

According the metallography of the produced AMSF blocks the unwanted porosity (between the matrix material and the hollow spheres) is negligible, but note that cracks in the wall of some spheres may occur, therefore some of these hollow spheres were maybe filled with matrix material during infiltration process. Detailed description of the metallographic investigations and properties of this types of AMSFs were already published [28, 40, 47, 48, 50] for visualization of the microstructures the three different grades of hollow spheres can be observed in Fig. 1. Both the small unwanted porosity and previously measured interfacial layers (~10 μm) indicating a good AMSF quality [48].

2.2 Compressive tests of the AMSFs

As it was mentioned in the Introduction, the main load type of the MMSFs is compression, also in sliding machine components. Therefore compressive test were performed on a MTS 810 universal materials testing machine on cylindrical samples with Ø14 mm diameter and 14 mm height. The specimens and the tools were lubricated with antiseize material with MoS_2 content. The compression tests were made in quasi-static condition with 0.01 s^{-1} deformation rate. Minimum number of 6 specimens were tested and the average characteristic values were determined according to the DIN 50134:2008 standard. The investigated characteristic properties were the structural stiffness (S), the fracture strain (ε_c), the compressive strength (σ_c), the yield strength (σ_y), the plateau strength (σ_p), the fracture energy (W_c) and the absorbed energy ($W_{25\%}$). In the compressive stress–strain curve of AMSFs (engineering system), S is the slope of the initial curve, where the whole system is deformed only elastically. σ_c is the stress value of the first local peak in the stress–strain curve where the breakage (ceramic) and plastic deformation (iron) of the hollow spheres begin. σ_y was determined at 1 % plastic strain, after this stress value the densification of the foam begins, the ceramic hollow spheres brake into smaller pieces the iron ones deform plastically and the plastically deformed matrix material fills the hollow spaces. In these densification region σ_p was determined as the mean value between ε = 5–25 % deformation. The fracture energy

(W_c) is the integral (area under the curve) of the stress–strain curve up to the fracture strain (ε_c, as the abscissa of σ_c) and the absorbed energy ($W_{25\%}$) is the integral up to the end of the test (ε = 25 %). Note that the 100GM-0GC specimens had no local peak in the stress–strain curve, therefore in this case the σ_c value was replaced by σ_y [48].

2.2 Pin-on-disc tribological tests

For the investigation of the tribological behavior of the produced hybrid AMSFs, pin-on-disc tests were performed. The pins were machined from the AMSF blocks with Ø 14 mm diameter and 20 mm height. The sliding surfaces of the specimens were grinded on SiC grinding papers (till P2400 paper) under continuous water rinsing. The carbon steel counterpart disc (1.0244) was Ø 100 mm, with the chemical composition of 98.4 wt.% Fe, 0.221 wt.% C, 0.211 wt.% Si, 0.913 wt.% Mn, 0.0697 wt.% Cr, 0.275 wt.% other. The surfaces of the discs were ground to an average surface roughness of R_a = 0.93 ± 0.321 µm and R_z = 8.74 ± 3.00 µm with the hardness of 140±3 HV10. Directly prior to the wear tests both the surface of the specimens and the discs were cleaned with acetone and ethanol. For the tribological tests a custom made pin-on-disc machine [42] was used. The machine parameters were: (I) 98 N load generating 0.64 MPa nominal surface pressure, (II) sliding speed was 0.2 m s^{-1}. The tests were made in dry and lubricated conditions at ambient temperature. Before the lubricated the test 5 × 20 µl 10W40 mineral oil was applied on the surface of the discs along the sliding track and no further lubrication was added up to the end of tests. For more details, refer to our previous paper [41]. The following parameters were determined in dry and lubricated conditions for all the AMSFs and matrix material: COF in the steady state (determined with Origin software as an average value between 300-500m sliding distance) (μ_{SS}), specific wear in the steady state (determined between 300-500m sliding distance) (v_{SS}), overall height loss of the specimens until 500 m sliding distance (Δh_{500m}), and the difference of the surface roughness of the discs (ΔR_a and ΔR_z) before and after the pin-on-disc test (the R_a, R_z values of the discs after the sliding tests were substracted from the initial R_a, R_z values of the discs before the tests) . The surface roughness of the discs was measured with a Mitutoyo SJ-201P surface roughness tester according to the ISO 4287:1997 standard. To investigate the effect of the reinforcement size, type and ratio on the worn surfaces and subsurface areas light microscope images were taken from the worn surfaces and in cross section of the specimens, all the detailed metallography images and their evaluation were also introduced in our previous work [41]. In dry condition the average wear groove depth and width (W_{depth} and W_{width}) and also the deformed material depth ($W_{deformed}$) of AMSF pin specimens were measured. Note that, in lubricated conditions, the traces of the pin were too small and shallow to measure.

In this article we show the connection between the tribological results and the compressive mechanical properties and the density of the hybrid AMSFs for further materials design and selection.

3. Results and discussion

Some correlations between different material parameters such as density – compressive properties – and tribological properties were determined, the type and parameters of the correlation are all listed in Table 1. Because of the generally large scatter of the tribological data, we call "good correlation" the cases where the coefficient of determination (R^2) of the fitted function was above $R^2 \geq 0.8$, for further evaluation only these correlations were discussed.

3.1 Mechanical properties

The measured densities (ρ_{AMSF}) of the AMSF blocks and the matrix material, determined by Archimedes' method, are from 100 GM to 100 GC reinforcement 1.38, 1.64, 1.65, 1.69, 1.74, 1.83 gcm^{-3}, the densities of SLG+GC, SLG and matrix material were 1.62, 1.38 and 2.65 gcm^{-3} respectively. The densities of our AMSFs are considerably lower, than the similar AMSFs investigated in the literature [30–38] (where ρ_{AMSF}>1.9 gcm^{-3}).

The quasi-static compression tests showed significant difference in the characteristic properties of the AMSFs. Due to the higher elastic modulus of the ceramic hollow spheres compared to the iron ones the structural stiffness of the GM-GC hybrid AMSFs increased significantly with higher GC content from 2369 MPa to 4405 MPa, the pure SLG specimen had only 2054 MPa structural stiffness, but in the SLG+GC hybrid it increased to 4123 MPa.

The compressive strength of GM-GC hybrids increased from 35.3 MPa to 114.5 MPa due to the greater load bearing capability of the ceramic GC hollow spheres. The SLG foams had significantly higher compressive strength (164 MPa) due to the smaller diameter of the ceramic spheres, which decreased in case of SLG+GC foam because of the bimodal distribution of the spheres and significantly less matrix material between them. The same effect can be observed in case of yield strength and plateau strength values. The plateau strength increased from 49.3 MPa to 88.1 MPa in case of GM-GC hybrids, and decreased from 150 MPa (SLG) to 94.8 MPa in case of SLG+GC hybrid. Also the plateau strength increased from 49.3 MPa to 88.1 MPa in case of GM-GC hybrids, and decreased from 111 MPa (SLG) to 26 MPa in case of SLG+GC hybrid.

In case of GM-GC type AMSFs linear correlation was established between the density – structural stiffness, and the density – strength values (σ_c, σ_y and σ_p), respectively (Figs. 2a), 2c) and Table 2).

Because of the significant increase of the strength values, the absorbed energy values also increased with the higher ceramic content (from 11.3 Jcm^{-3} to 19.6 Jcm^{-3}) in case of the GM-GC hybrids and decreased from 25.5 Jcm^{-3} (SLG) to 9.5 Jcm^{-3} in case of SLG+GC hybrid. In the case of GM-GC AMSFs linear correlation was detected between the density – absorbed energy values (Fig. 2e and Table 2).

During compressive loading the ceramic type GC and SLG hollow spheres had no plastic deformation, the AMSFs simply ruptured along a shear plane closing 45° to the loading direction (the other parts of the specimen were almost unharmed). Compared to this, the pure iron GM spheres (they are also polycrystalline with grain size <10 μm [50]) can bear large plastic deformation. This plastic deformation becomes dominant, resulting diffuse plastic deformation of the whole specimen. It was typical in the GM-GC hybrid AMSFs from at least 80 vol.% GM grade reinforcement. Therefore the fracture strain decreased from 6% to 3.2% with increasing GC content in the GM-GC hybrids. The pure SLG specimen had larger fracture strain (9.6%) – because of the small sphere size –, and it decreased with the addition of larger ceramic hollow spheres in the SLG+GC hybrid. The SLG AMSF also had the highest fracture energy and absorbed energy which decreased in the SLG+GC specimens and in case of GM-GC hybrids they had a minimum at 40GM-60GC reinforcement due to the complex effect of the above detailed strength and strain behavior. A good fitting of a polynomial function was found for both density – fracture energy and density – fracture strain values (Figs. 2b), 2d) and Table 2).

3.2 Tribological properties

From the test results of our previous work [40, 41], the following conclusions were drawn, which are the fundamentals of the present article about the trends between tribological results and material properties of AMSFs. In dry sliding conditions: (I) In case of GM-GC hybrid AMSFs the COF increased with the ceramic reinforcement, the SLG+GC AMSF showed the highest COF. (II) In steady-state the specific wear and the overall height loss of the specimens increased with the ceramic hollow sphere content. (III) the wear type was mainly abrasive caused by the broken, hard ceramic particles (in the wear debris) beside the metallic adhesion and depended strongly on the amount and size of ceramic particles of the broken GC and SLG hollow spheres. This ceramic particle amount increased with the higher volume fraction of GC reinforcement of the AMSFs. It was also observed, that most of the larger sized GM and GC type hollow spheres were filled with debris and plastically deformed matrix material. In oil lubricated sliding conditions: (I) The COF was significantly less and in case of GM-GC hybrid AMSFs it slightly decreased with the higher ceramic reinforcement content, and was less than the bulk matrix material. (II) the specific wear values were two orders of magnitude smaller, the height loss of the specimens were one order of magnitude smaller, compared to dry friction. (III) all hollow sphere grades remained open and acted as lubricant reservoirs and dispensers. The surfaces of the specimen became smoother and the wear discs also showed no significant wear tracks.

Although the AlSi12 matrix material had less wear rate and height loss compared to the AMSFs in dry condition, in lubricated conditions the obtained values were really close to some hybrid specimen, despite they have significantly less real contact surface.

The exact values of the characteristic tribological parameters determined in dry and lubricated conditions were further evaluated and correlations between the different mechanical properties were established.

3.3. Correlations between mechanical and tribological properties

The tribological parameters were plotted in the function of the compressive mechanical parameters Fig. 4-6. With Origin software (e.g. Fig. 3-4 as function of the structural stiffness) correlations were searched. Table 1 lists the properties where good correlations could be found. Table 2 lists the parameters of the established correlation. The possible correlation between the mechanical and tribological properties often helps to predict the behaviour of different materials under a given condition [42].

The defined connections can be well explained on the basis of the adhesion theory of friction [51], the dry friction force F_f is equal to the sum of adhesion (F_a) and deformation (F_d) components, $F_f=F_a+F_d$. Concerning the wear mechanism the combination of adhesive, abrasive, and third body effects play role. The detailed evaluations are as follow.

In Fig. 3-4 the significant difference between the dry and lubricated conditions of the sturctural stiffness – tribological parameters can be observed.

In dry condition the increase of the structural stiffnes also increases the COF (μ_{SS}) and the specific wear values in the steady state (v_{SS}). This occured due to the fact, that under the given nominal load in the real contact zone the deformation of the specimes with higher S values was less (more harder ceramic GC hollow spheres with greater wall tickness), therefore beside the adhesion on the relatively smaller contact surface of the asperities, the deformation component of the less deformed microgeometry became dominant. This caused significant stress concentration in the real contact zone, which resulted in breaking off the porous specimen surface (more and more hard ceramic GC content), increasing the wear rate. The increased wear caused partially third-body abrasion also in the surface of the steel counterpart. This effect also reflects in the trends of the wear groove depth and width values determined on metallographic images. A decreasing trend (but not a good correlation) of deformed zone also can be seen because of the more stiff specimen and less contact zone.

As a function, between $S - \mu_{SS}$ and $S - v_{SS}$ linear correlation while between $S - \Delta h_{500m}$ lognormal correlation was established (Tables 1 and 2).

In lubricated condition the stiffer contact zone (due to the higher ceramic hollow sphere content with higher hardness and Young modulus) was beneficial, because the porosities could hold the lubrication better with less deformation than the surfaces with less structural stiffness therefore with larger deformation. The better lubrication caused also less contact stress and wear.

As a function, between $S - \mu_{SS}$ linear, and between $S - v_{SS}$ exponential decay correlation was found to fit the best (Tables 1 and 2).

The structural stiffnes had no distinctive effect on the changes in the surface roughness of the discs (ΔR_a and ΔR_z) neither in dry nor in lubricated condition (Figs. 3 and 4).

For further visualisation only the graphs with good correlation between mechanical and tibological parameters are plotted (Figs. 5 and 6).

In case **of dry sliding** a linear correlation can be observed between the density and height loss values of the GM-GC hybrids (Fig. 5a). The increasing ceramic hollow sphere content – with higher density – decreased the overall height loss. It can be explained by the resultant effect of the greater adhesion in the contact zone and the auxilary abrasion mechanisms.

Moreover in case of GM-GC hybrid AMSFs the increase of the fracture strain decreased the COF (Fig. 5c): an exponential correlation was found. In the investigated system, at the given load and sliding speed the deformation component of the friction decreased because of the smaller plasicity (more GC with higher hardness, Young modulus and crush strength), while the adhesion component did not increased significantly. The increase in the fracture strain at the same time also decreased the wear and the number of detached particles from the specimens. Between σ_c and Δh_{500m} linear correlation was observed (Fig. 5e). In the aspect of wear the yield strength has a distinct effect too. In case of GM-GC hybrids the σ_c – v_{SS} values as well as the σ_c – Δh_{500m} showed a polinomial correlation, where the values have a maxima at about σ_c = 90 MPa.

In oil lubricated conditions some correlations between tribological and mechanical properties can be established as follows (Figs. 5 and 6). Investigating either the friction or the wear it can be confirmed, that behind the detected trends the developed, sustained and efficient lubrication is decisive. The development of an efficient lubrication is a really complex process between (different) contact surfaces with different porosity, microgeometry, adhesive aptitude and deformability. The dominant factors of the investigated systems can be observed in Figs. 5 and 6.

The COF decreasing effect of the higher density indicates more adherent lubrication on the contact surface (on the thicker walls of the GC grade hollow spheres). A polinomial correlation between ϱ_{AMSF} and μ_{SS} was found (Fig. 5b). While with increasing fracture strain the COF also increases because of the higher deformation work (more plastically deformable iron hollow spheres GM in the AMSFs) increasing the friction. Between σ_{c} and μ_{SS} exponential correlation was observed (Fig. 5d). In case of GM-GC hybrids the increase of the yield strength decreased the resultant friction (Fig. 6b). The lubrication film minimalizes the adhesion, and the deformation component (more hard ceramic GC hollow spheres in the AMSFs, with higher hardness yield strength) of the friction decreased with higher yield strength of the AMSFs therefore decreasing the resultant friction. Similar observations can be made in case of yield strength-specific wear (Fig 6d) and plateau strength-COF relations Fig 6e. In all cases ($\sigma_{\mathrm{y}} - \mu_{\mathrm{SS}}$, $\sigma_{\mathrm{y}} - v_{\mathrm{SS}}$, $\sigma_{\mathrm{p}} - \mu_{\mathrm{SS}}$) linear correlation was established for the GM-GC hybrid AMSFs.

The GC+SLG hybrid specimen usually differs from the other AMSFs because of its bimodal hollow sphere distribution, the real contact surface area is a lot smaller and there is significantly less matrix material between the different hollow spheres. Therefore the ceramic hollow spheres can detach from the surface easier thus increases the third body abrasion. Also the wall thickness differs in two order of magnitude. In case of the SLG samples the real contact surface is also different and the distance between hollow sphere and matrix material (surface cavity distribution) much less than in the case of the AMSFs reinforced with GM-GC spheres. The effects of these facts performed often strongly diffeing tribological behaviour comapring to GC – GM composites.

4. Conclusions

The previously obtained (by pin-on-disc tests) [41] tribological properties of AlSi12 matrix GM-GC and SLG reinforced hybrid AMSFs were investigated in comparison with their density and quasi-static compressive properties [48]. In many cases good correlation (R^2>0.8) was found between the investigated parameters. The phenomena were explained on complex basis of the adhesion theory of friction, the mechanical properties of composite surfaces, the adhesive and abrasive wear mechanism altogether. From the test results and in the aspect of materials selection for mechanically loaded sliding machine parts the following conclusions can be drawn:

- In case of GM-GC AMSFs density correlated linearly with the structural stiffness, the fracture strength, the yield strength, the plateau strength and the absorbed energy values, respectively. A good polynomial correlation of second degree was also found between the density – fracture strain and fracture energy values. All of the before mentioned properties increased with higher density, except the fracture strain and absorberd energy values.

As for the correlations with tribological properties **in dry sliding** conditions:

- With higher structural stiffness of the AMSFs the COF and specific wear increased linearly and the overall height loss increased with a lognormal function.
- With higher density, the overall height loss increased linearly.
- With higher fracture strain values the COF decreased exponentially and the overall height loss decreased linearly.
- Between the yield strength – height loss and specific wear values a second order polynomial correlation was established.

As for the correlations with tribological properties **in oil lubricated sliding** conditions:

- In case of GM-GC AMSFs with higher structural stiffness the COF decreased linearly, while the specific wear decreased exponentially.
- A second order polynomial decrement was established in the COF with higher AMSFs density.
- Higher fracture strain increased the COF exponentially.
- In the case of GM-GC AMSFs with higher strength values (compressive, yield and plateau strength too) the COF decreased linearly.
- With higher yield strength the specific wear decreased linearly in case of the GM-GC hybrids.

The GC+SLG hybrid samples significantly differs from the other AMSFs, therefore usually showed different tribological and mechanical properties. The main reason of this phenomena can be found in their bimodal hollow sphere distribution. In this case the real contact surface area is a lot smaller and there is a significantly less matrix material between the different hollow spheres.

Altogether these results enlighten the basic trends and correlations between mechanical and sliding characteristics of hybrid composites and enable to tailor not only for the mechanical but for the tribological properties as well for further development and application of AMSFs.

Acknowledgements

This paper was supported by the János Bolyai Research Scholarship of the Hungarian Academy of Sciences (L. Zsidai, grant number: BO/00127/13/6 and I.N. Orbulov, grant number: BO/00294/14).

References

[1] Gupta N and Rohatgi KP. Metal Matrix Syntactic Foams, DEStech Publications, Inc., Lancaster, Pennsylvania, USA, (2014) p 352. ISBN 978-1-932078-83-1

[2] Luong DD. Strbik OM. Hammond VH. Gupta N and Cho K. Development of high performance lightweight aluminum alloy/SiC hollow sphere syntactic foams and compressive characterization at quasi-static and high strain rates. J Alloys Compounds 550 (2013) 412.
DOI: 10.1016/j.jallcom.2012.10.171

[3] Santa Maria JA. Schultz BF. Ferguson JB. Guptan N. and Rohatgi PK. Effect of hollow sphere size and size distribution on the quasi-static and high strain rate compressive properties of Al-A380-Al2O3 syntactic foams. J. Mater Sci. 49 (2014) 1267.
DOI: 10.1007/s10853-013-7810-y

[4] Rohatgi PK. Gupta N. Schultz BF. and Luong DD. The synthesis, compressive properties, and applications of metal matrix syntactic foams. JOM 63(2) (2011) 36.
DOI: 10.1007/s11837-011-0026-1

[5] Luong DD. Gupta N. Daoud A. and Rohatgi PK. High strain rate compressive characterization of aluminum alloy/fly ash cenosphere composites. JOM 63(2) (2011) 53.
DOI: 10.1007/s11837-011-0029-y

[6] Luong DD. Gupta N. and Rohatgi PK. The high strain rate compressive response of Mg-Al alloy/fly Ash cenosphere composites. JOM 63(2) (2011) 48. 10.1007/s11837-011-0028-z

[7] Cox J. Luong DD. Shunmugasamy VC. GuptaN. Strbik III OM. and Cho K. Dynamic and Thermal Properties of Aluminum Alloy A356/Silicon Carbide Hollow Particle Syntactic Foams. Metals 4 (2014) 530.
DOI: 10.3390/met4040530

[8] Rabiei A. and Garcia-Avila M. Effect of various parameters on properties of composite steel foams under variety of loading rates. Mater Sci Eng A 564 (2013) 539.
DOI: 10.1016/j.msea.2012.11.108

[9] Alvandi-Tabrizi Y. Whisler DA. Kim H. and RabieiA. High Strain Rate Behavior of Composite Metal Foam. Mater Sci Eng A 631 (2015) 248.
DOI: 10.1016/j.msea.2015.02.027

[10] Alvandi-Tabrizi Y. and RabieiA. Use of Composite Metal Foam for Improving Absorption of Collision Forces. Procedia Mater Sci. 4 (2014) 377.
DOI: 10.1016/j.mspro.2014.07.577

[11] Taherishargh M. Belova IV. Murch GE. and Fiedler T. Low-density expanded perlite-aluminium syntactic foam. Mater Sci Eng A. 64 (2014) 127.
DOI: 10.1016/j.msea.2014.03.003

[12] Taherishargh M. Belova IV. Murch GE. and FiedlerT . On the mechanical properties of heat-treated expanded perlite–aluminium syntactic foam. Mater Des 63 (2014) 375.
DOI: 10.1016/j.matdes.2014.06.019

[13] Taherishargh M. Sulong MA. Belova IV. Murch GE. and Fiedler T. On the particle size effect in expanded perlite aluminium syntactic foam. Mater Des. 66 (2015) 294.
DOI: 10.1016/j.matdes.2014.10.073

[14] Taherishargh M. Belova IV. Murch GE. and Fiedler T. Pumice/aluminium syntactic foam. Mater Sci Eng A. 635 (2015) 102.
DOI: 10.1016/j.msea.2015.03.061

[15] Fiedler T. Taherishargh M. Krstulović-Opara L. and Vesenjak M. Dynamic compressive loading of expanded perlite/aluminum syntactic foam. Mater Sci Eng A. 626 (2015) 296.
DOI: 10.1016/j.msea.2014.12.032

[16] Taherishargh M. Vesenjak M. Belova IV. Krstulović-Opara L. Murch GE. and Fiedler T. In situ manufacturing and mechanical properties of syntactic foam filled tubes. Mater & Des. 99 (2016) 356.
DOI: 10.1016/j.matdes.2016.03.077

[17] Weise J. Lehmhus D. Baumeister J. Kun R. Bayoumi M. and Busse M. Production and Properties of 316L Stainless Steel Cellular Materials and Syntactic Foams. Steel Res Int. 85(3) (2014) 486.
DOI: 10.1002/srin.201300131

[18] Peroni L. Scapin M. Avalle M. Weise J. and Lehmhus D. Dynamic mechanical behavior of syntactic iron foams with glass microspheres. Mater Sci Eng A. 522 (2012) 364.
DOI: 10.1016/j.msea.2012.05.053

[19] Lehmhus D. Weise J. Baumeister J. Peroni L. Scapin M. Fichera C. Avalle M. and Busse M. Quasi-static and Dynamic Mechanical Performance of Glass Microsphere- and Cenosphere-based 316L Syntactic Foams. Procedia Mater Sci. 4 (2014) 383.
DOI: 10.1016/j.mspro.2014.07.578

[20] Peroni L. Scapin M. Fichera C. Lehmhus D. Weise J. Baumeister J. and Avalle M. Investigation of the mechanical behaviour of AISI 316L stainless steel syntactic foams at different strain-rates. Composites Part B. 66 (2014) 430.
DOI: 10.1016/j.compositesb.2014.06.001

[21] Castro G. and Nutt SR. Synthesis of syntactic steel foam using gravity-fed infiltration. Mat Sci Eng A-Struct 553 (2012) 89.
DOI: 10.1016/j.msea.2012.05.097

[22] Castro G. and Nutt SR. Synthesis of syntactic steel foam using mechanical pressure infiltration. Mater Sci Eng A. 535 (2012) 274.
DOI: 10.1016/j.msea.2011.12.084

[23] Goel MD. Peroni M. Solomos G. Mondal DP. Matsagar VA. Gupta AK, Larcher M. and Marburg S. Dynamic compression behavior of cenosphere aluminum alloy syntactic foam. Mater Des. 42 (2012) 418.
DOI: 10.1016/j.matdes.2012.06.013

[24] Goel MD. Mondal DP. Yadav MS. and Gupta AK. Effect of strain rate and relative density on compressive deformation behavior of aluminum cenosphere syntactic foam. Mater Sci Eng A. 590 (2014) 406.
DOI: 10.1016/j.msea.2013.10.048

[25] Goel MD. Matsagar VA. Gupta AK and Marburg S. Strain rate sensitivity of closed cell aluminum fly ash foam. Trans Nonferrous Metals Soc China 23()4 (2013) 1080.
DOI:10.1016/S1003-6326(13)62569-8

[26] Xue X-B. Wang L-Q. Wang M-M. Lü W-J. and D. Zhang. Manufacturing, compressive behaviour and elastic modulus of Ti matrix syntactic foam fabricated by powder metallurgy. Trans Nonferrous Metals Soc China. 22 (2012) 188.
DOI:10.1016/S1003-6326(12)61707-5

[27] Xue X-B. and ZhaoY. Ti matrix syntactic foam fabricated by powder metallurgy: Particle breakage and elastic modulus. JOM 63(2) (2011) 43.
DOI:10.1007/s11837-011-0027-0

[28] Orbulov IN. Májlinger K. Microstructural aspects of ceramic hollow microspheres reinforced metal matrix composites. Int. J Mater. Res. 9 (2013) 903
DOI: 10.3139/146.110944

[29] Kozma I. Zsoldos I. Dorogi G. and Papp S. Computer tomography based reconstruction of metal matrix syntactic foams. Per Pol Mech. Eng. 58 (2014) 87.
DOI: 10.3311/PPme.7337

[30] Rohatgi PK. and Guo RQ. Mechanism of abrasive wear of Al-Si hypoeutectic alloycontaining 5 vol% fly ash. Trib. Lett. 3 (1997) 339.
DOI: 10.1023/a:1019109911923

[31] Ramachandra M. and Radhakrishna K. Synthesis-microstructure-mechanical properties-wear and corrosion behavior of an Al-Si (12%)—Flyash metal matrix composite. J. Mat. Sci. 40 (2005) 5989.
DOI: 10.1007/s10853-005-1303-6

[32] Ramachandra M. and Radhakrishna K. Effect of reinforcement of flyash on sliding wear, slurry erosive wear and corrosive behavior of aluminium matrix composite. Wear 262 (2007) 1450.
DOI: 10.1016/j.wear.2007.01.026

[33] Mondal DP. Das S. and Jha N. Dry sliding wear behaviour of aluminum syntactic foam. Mat. & Des. 30 (2009) 2563-2568.
doi:10.1016/j.matdes.2008.09.034

[34] Uthayakumar M. Thirumalai Kumaran S. and Aravindan S. Dry Sliding Friction and Wear Studies of Fly Ash Reinforced AA-6351 Metal Matrix Composites. Advances in Tribology (2013) 1.
DOI: 10.1155/2013/365602

[35] Sudarshan MKS. Dry sliding wear of fly ash particle reinforced A356 Al composites. Wear 265 (2008) 349.
DOI: 10.1016/j.wear.2007.11.009

[36] Saravanan V. Thyla PR. and Balakrishnan SR. The dry sliding wear of cenosphere-aluminum metal matrix composite. Adv. Comp. Lett. 23(3) (2015) 49.
WOS:000348172800001

[37] Kumar KAR. Balamurugan K. and Gnanaraj D. Hardness, Tribology and Microstructural studies on Aluminium – Flyash metal Matrix Composites. J.

Scientific & ind. Res. 74(3) (2015) 165.

WOS:000351023600007

[38] Kumar V. Gupta RD. and Batra NK. Comparison of Mechanical Properties and Effect of Sliding Velocity on Wear Properties of Al 6061, Mg 4%, Fly Ash and Al 6061, Mg 4%, Graphite 4%, Fly Ash Hybrid Metal Matrix Composite. Procedia Mat. Sci. 6 (2014) 1365

DOI: 10.1016/j.mspro.2014.07.116

[39] Muthu P. and Rajesh S. Dry Sliding Wear Behaviour of Aluminum/Sic/Flyash Hybrid Metal Matrix Composites. J Australian Cer Soc. 52(1) (2016) 125.

WOS:000367924100020

[40] Májlinger K. Wear properties of hybrid AlSi12 matrix syntactic foams . Int. J Mater. Res.106(11) (2015) 1165.

DOI:10.3139/146.111290

[41] Májlinger K. Bozóki B. Kalácska G. Keresztes R. and Zsidai L. Tribological properties of hybrid aluminum matrix syntactic foams. Trib Int. 99 (2016) 211.

DOI: 10.1016/j.triboint.2016.03.032

[42] Kalácska G. An engineering approach to dry friction behaviour of numerous engineering plastics with respect to the mechanical properties. Exp Pol Lett 7(2) (2013)199

DOI: 10.3144/expresspolymlett.2013.18

[43] http://hollomet.com/produkte.html (last accessed on 2014.08.10.)

[44] http://www.envirospheres.com/products_bl.asp (last accessed on 2015.03.10.)

[45] Jaegerand HM. and Nagel SR. Physics of the Granular State. Science 255 (1992) 1523.
DOI: 10.1126/science.255.5051.1523

[46] Torquato S. Truskett TM. and Debenedetti PG. Is Random Close Packing of Spheres Well Defined? Phys. Rev. Lett. 84 (2000) 2064.
DOI: 10.1103/PhysRevLett.84.2064

[47] Orbulov IN. Metal matrix syntactic foams produced by pressure infiltration—The effect of infiltration parameters. Mat. Sci. & Eng. A 583 (2013)
DOI: 11. 10.1016/j.msea.2013.06.066

[48] Májlinger K. and Orbulov IN. Characteristic compressive properties of hybrid metal matrix syntactic foams. Mater Sci Eng A 606 (2014) 248.
DOI: 10.1016/j.msea.2014.03.100

[49] Ashby MF. Evans AG. Fleck NA. Gibson LJ. Hutchinson JW. and Wadley H N G. Metal Foams: A Design Guide, Butterworth-Heinemann, Boston (2010).
ISBN: 0750672196

[50] Szlancsik A. Katona B. Májlinger K. and Orbulov IN. Compressive Behavior and Microstructural Characteristics of Iron Hollow Sphere Filled Aluminum Matrix Syntactic Foams. Materials 8(11) (2015) 7926
DOI: 10.3390/ma8115432

[51] Bowden FP. and Tabor D. Friction and Lubrication of Solids, Oxford University Press, London, 1954.
ISBN: 9780198507772

Tables and their captions

Table 1. Matrix of the compared mechanical and tribological parameters with indication of the ones with good correlation.

Table 1 Matrix of the compared mechanical and tribological parameters with indication of the ones with good correlation

Physical and mechanical properties	Dry sliding condition								Oil-lubricated condition					Density ρ_{AMSF}
	COF μ_{SS}	Specific wear V_{SS}	Height loss Δh_{500m}	Difference in surface roughness of the disc		Wear grove width W_{width}	Wear grove depth W_{depth}	Deformation depth $W_{deform.}$	COF μ_{SS}	Specific wear V_{SS}	Height loss Δh_{500m}	Difference in surface roughness of the disc		
				ΔR_a	ΔR_z							ΔR_a	ΔR_z	
Structural stiffness, S	+	+	+	−	−	−	−	−	+	+	−	−	−	+
Density, ρ_{AMSF}	−	−	+	−	−	−	−	−	+	−	−	−	−	+
Compressive strength, σ_c	−	−	−	−	−	−	−	−	+	−	−	−	−	+
Fracture strain, ε_c	+	−	+	−	−	−	−	−	+	−	−	−	−	+
Fracture *energy, Wc*	−	−	−	−	−	−	−	−	−	−	−	−	−	+
Yield strength, σ_y	−	+	+	−	−	−	−	−	+	+	−	−	−	+
Plateau strength, σ_p	−	−	−	−	−	−	−	−	+	−	−	−	−	+
Absorbed energy, $W_{25\%}$	−	−	−	−	−	−	−	−	−	−	−	−	−	+

+ correlation ($R^2 \geq 0.8$)

− no correlation

Table 2. The equations and their parameters of the correlations between density – compressive properties – and tribological properties of the AMSFs.

Table 2 Equations and their parameters of the correlations between density andcompressive properties, and tribological properties of the AMSFs

Parameters		Equation of the correlation	Parameters of the equation						
1	2		a	SE	b	SE	y_0	SE	R^2
ρ_{AMSF}	S	$Y = a + b \cdot x$	−3616.1	795.77	4332.7	548.93			0.93
ρ_{AMSF}	σ_y	$Y = a + b \cdot x$	−189.4	34.49	159.4	21.20			0.92
ρ_{AMSF}	σ_c	$Y = a + b \cdot x$	−193.3	34.69	161.9	21.28			0.92
ρ_{AMSF}	σ_p	$Y = a + b \cdot x$	−64.7	14.58	81.2	8.95			0.94
ρ_{AMSF}	ε_c	$y = y_0 + a \cdot x^1 + b \cdot x^2$	−114.9	35.80	31.3	10.99	108.6	29.03	0.92
ρ_{AMSF}	W_c	$y = y_0 + a \cdot x^1 + b \cdot x^2$	−196.0	34.53	58.0	10.41	167.2	28.70	0.85
ρ_{AMSF}	$W_{25\%}$	$Y = a + b \cdot x$	−15.7	3.80	19.2	2.17			0.94
Dry condition									
S	μ_{SS}	$Y = a + b \cdot x$	0.381	0.011	$0.369 \cdot 10^{-5}$	$3.947 \cdot 10^{-6}$			0.95
S	v_{SS}	$y = a \cdot \exp(-x/b) + y_0$	−0.0308	0.019	$4.933 \cdot 10^{-5}$	$7.765 \cdot 10^{-6}$			0.87
S	Δh_{500m}	$y = y_0 + A/((2\pi)^{-2} \cdot a \cdot x)$	0.261	0.046	2129	61.4	0.671	0.012	0.99
		$\cdot \exp(-(\ln(x/b))^2/(2a^2))$		A	−477.1	18.3			
ρ_{AMSF}	Δh_{500m}	$Y = a + b \cdot x$	−0.726	0.262	0.784	0.161			0.79
ε_c	μ_{SS}	$y = a \cdot \exp(-x/b) + y_0$	0.432	0.322	5.659	21.1	0.301	0.702	0.83
ε_c	Δh_{500m}	$Y = a + b \cdot x$	0.859	0.025	−0.057	0.006			0.95
σ_y	v_{SS}	$y = y_0 + a \cdot x^1 + b \cdot x^2$	0.007	0.001	$-3.849 \cdot 10^{-5}$	$7.648 \cdot 10^{-6}$	−0.104	0.040	0.89
σ_y	Δh_{500m}	$y = y_0 + a \cdot x^1 + b \cdot x^2$	0.016	0.004	$-8.191 \cdot 10^{-5}$	$2.455 \cdot 10^{-5}$	−0.078	0.128	0.89
Lubricated condition									
S	μ_{SS}	$Y = a + b \cdot x$	0.138	0.004	$-1.341 \cdot 10^{-5}$	$1.767 \cdot 10^{-6}$			0.90
S	v_{SS}	$y = a \cdot \exp(-x/b) + y_0$	34,006	44,440	227.4	28.3	0.065	0.021	0.99
ρ_{AMSF}	μ_{SS}	$y = y_0 + a \cdot x^1 + b \cdot x^2$	0.537	0.329	−0.195	0.104	−0.261	0.258	0.82
σ_c	μ_{SS}	$Y = a + b \cdot x$	0.124	0.006	$-4.298 \cdot 10^{-4}$	$8.103 \cdot 10^{-5}$			0.84
ε_c	μ_{SS}	$y = a \cdot \exp(-x/b) + y_0$	−2.180	3.054	0.786	0.269	0.107	0.004	0.88
σ_y	μ_{SS}	$Y = a + b \cdot x$	0.124	0.005	$-4.378 \cdot 10^{-4}$	$7.411 \cdot 10^{-5}$			0.87
σ_y	v_{SS}	$Y = a + b \cdot x$	1.930	0.220	−0.0254	0.003			0.91
σ_p	μ_{SS}	$Y = a + b \cdot x$	0.154	0.013	$-9.123 \cdot 10^{-4}$	$1.919 \cdot 10^{-4}$			0.81

Figures and their captions

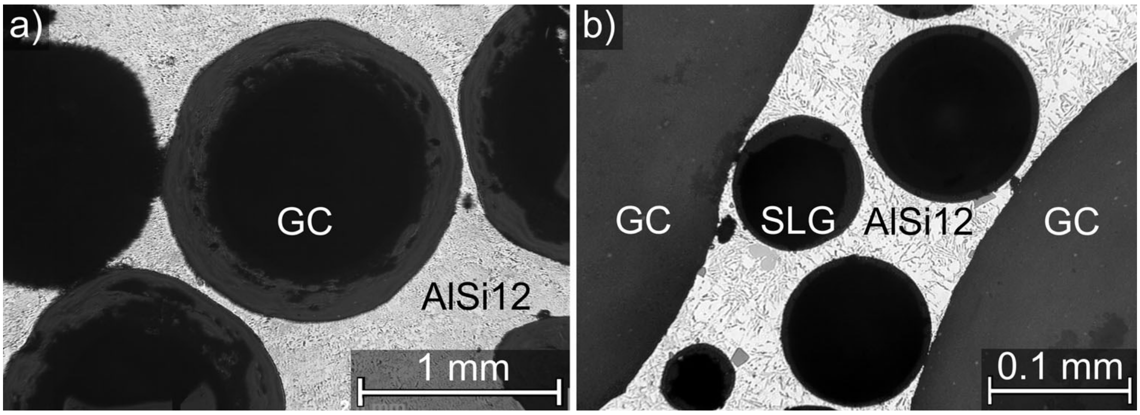

Figure 1. Optical microscope micrographs a) of the 80GM-20GC specimens and b) of the SLG+GC specimens microstructure

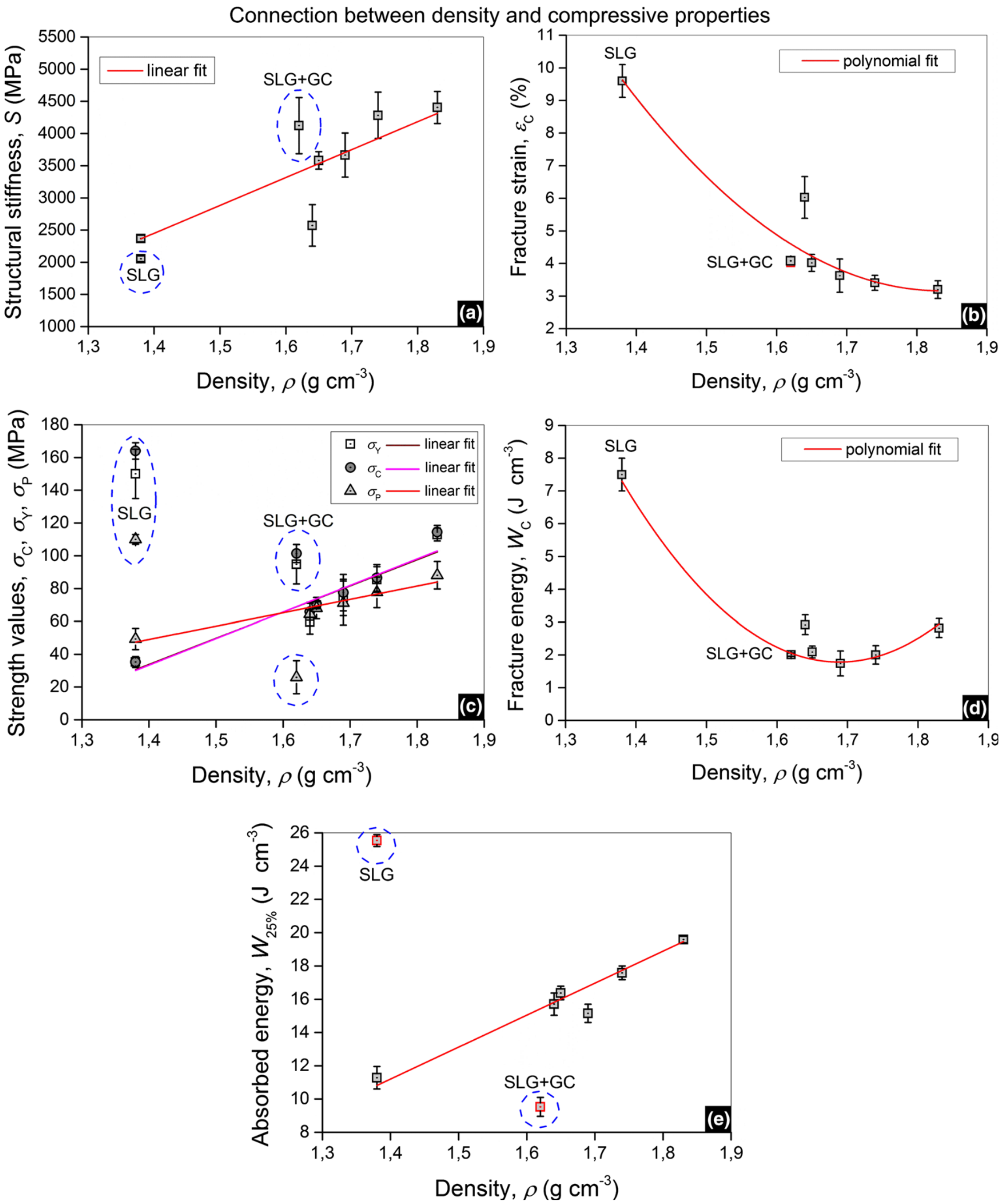

Figure 2. Correlations between the density and compressive properties; a) structural stiffness, b) fracture strain, c) compressive strength, yield strength and plateau strength d) fracture energy and e) absorbed energy of the AMSFs. Note, that the circled (dashed blue) SLG and SLG+GC specimens were not taken into account for the fitting.

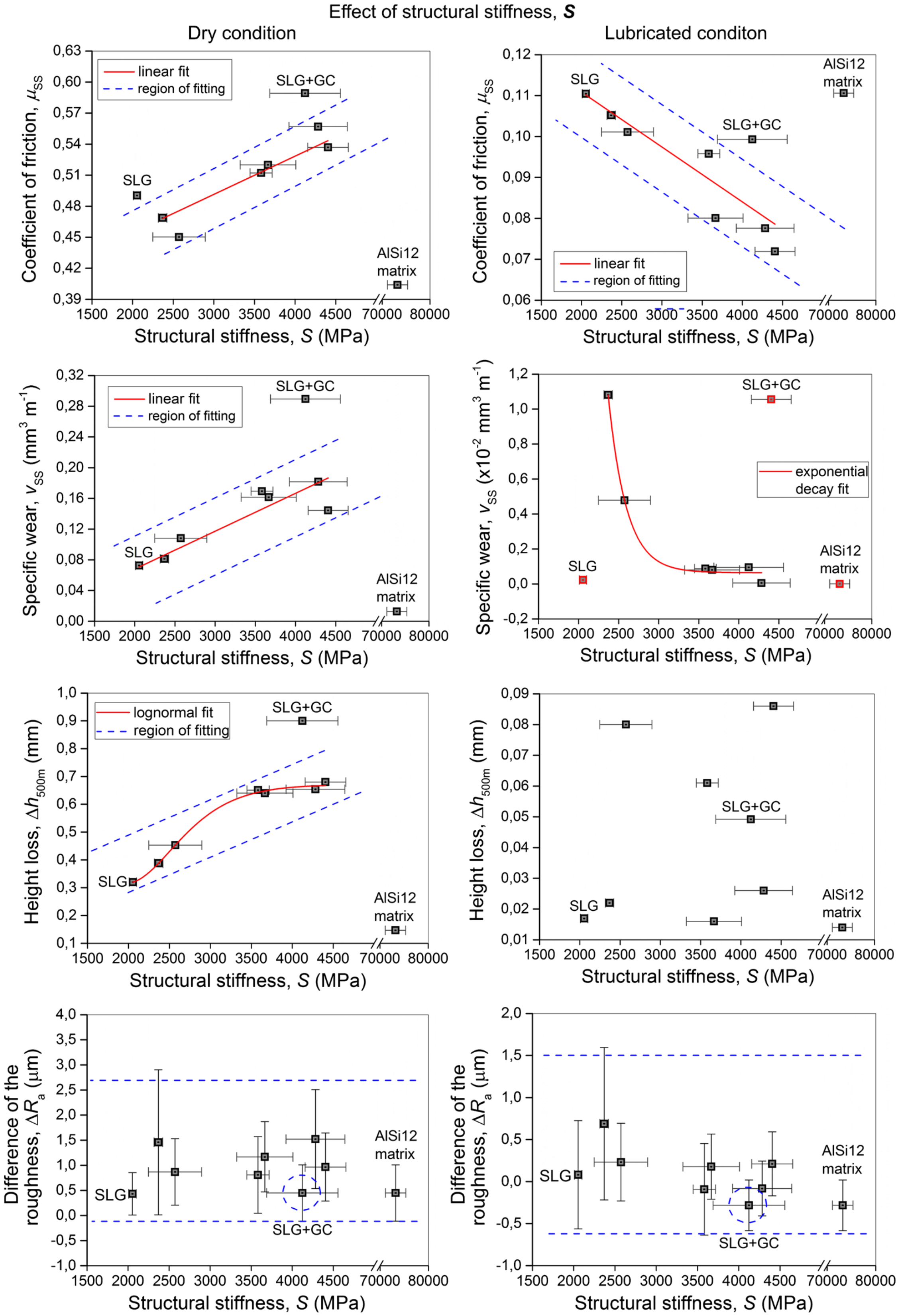

Figure 3. Correlation between the structural stiffness and the properties of the AMSFs determined with pin-on-disc tests in dry and lubricated conditions.

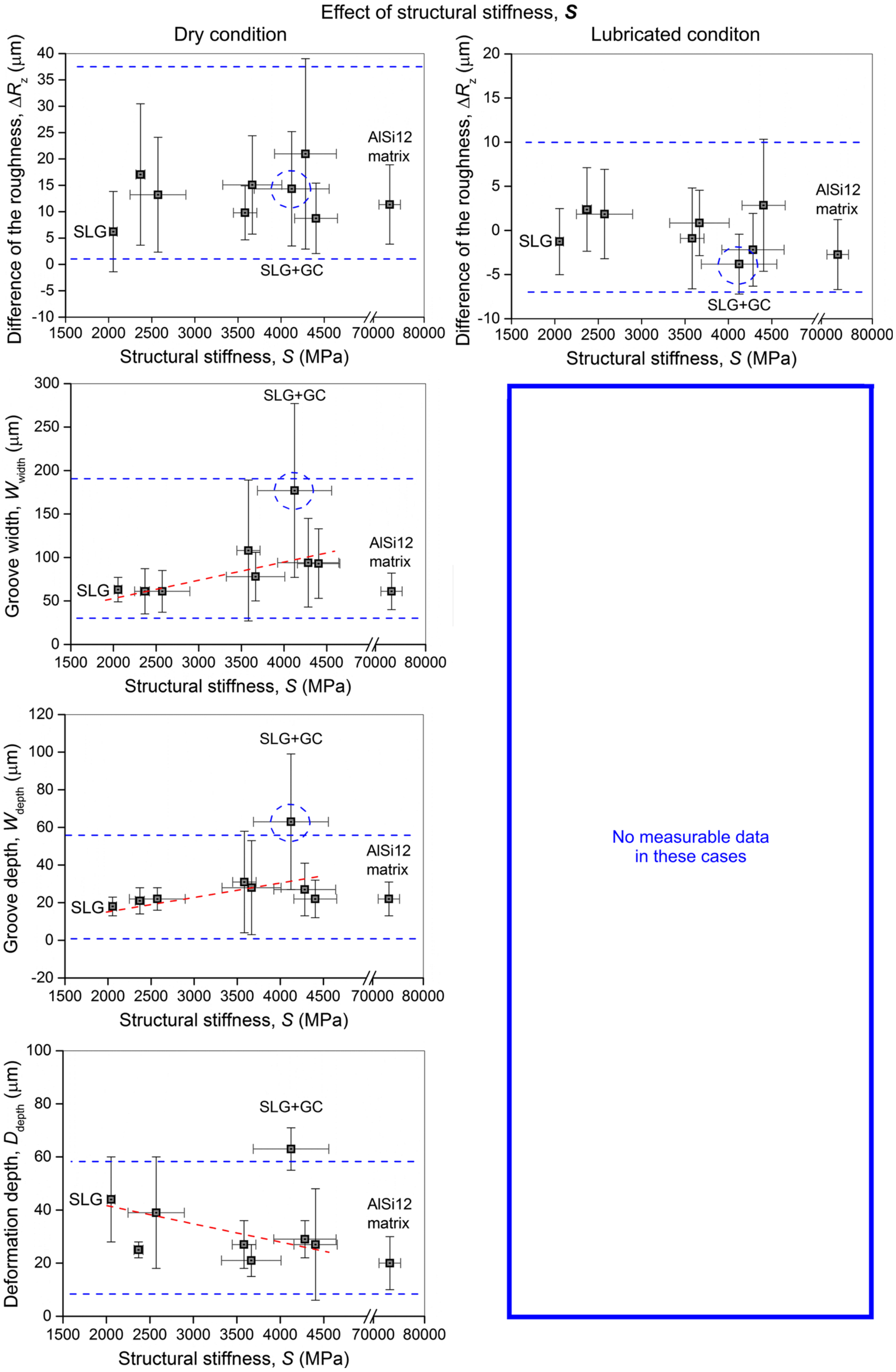

Figure 4. Correlation between the structural stiffness and the properties of the AMSFs determined with pin-on-disc tests in dry and lubricated conditions.

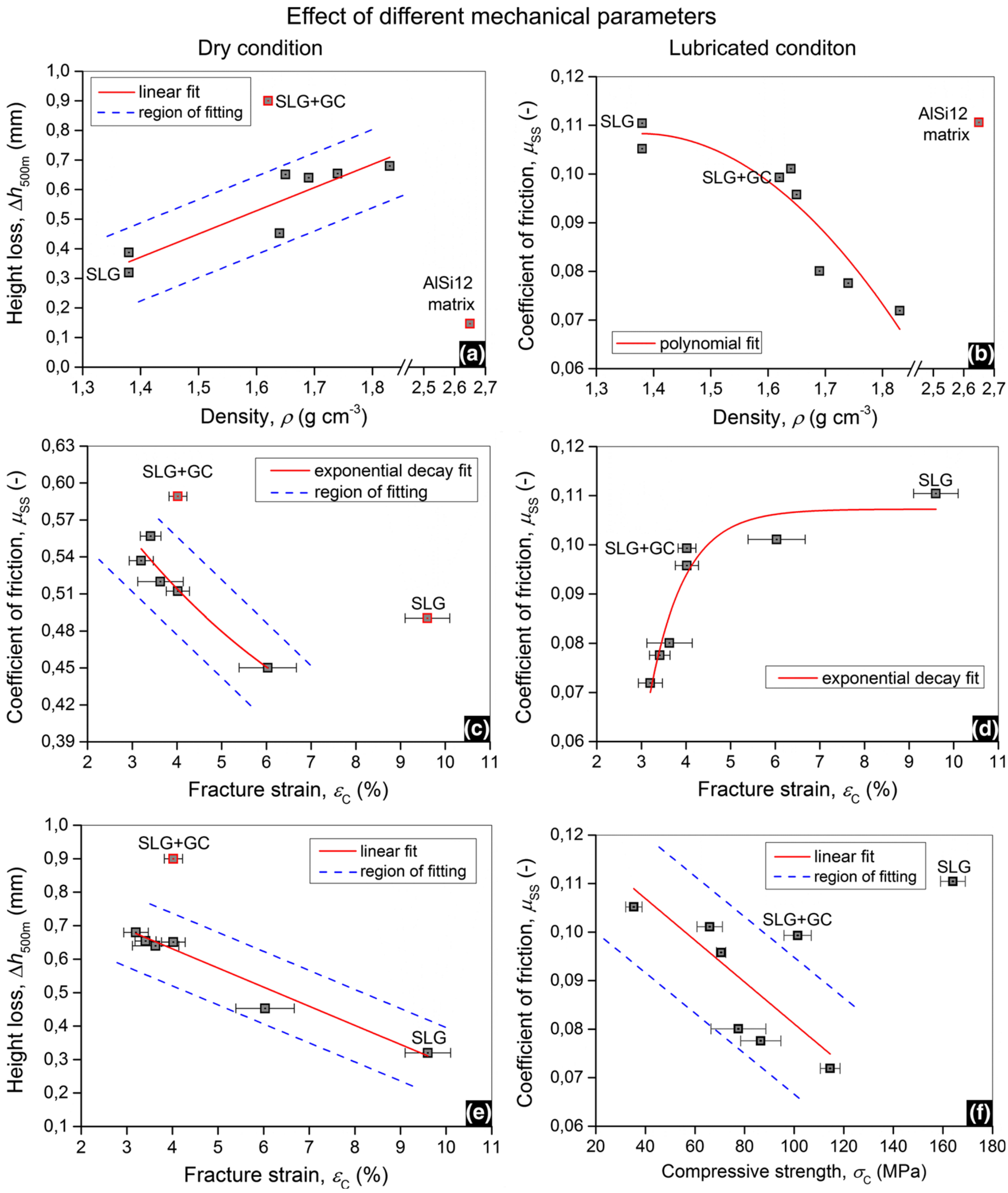

Figure 5. Correlation between; a) $\varrho - \Delta h_{500\text{m}}$, c) $\varepsilon_{\text{c}} - \mu_{\text{SS}}$, e) $\varepsilon_{\text{c}} - \Delta h_{500\text{m}}$ in dry condition and between; b) $\varrho - \mu_{\text{SS}}$, d) $\varepsilon_{\text{c}} - \mu_{\text{SS}}$, f) $\sigma_{\text{c}} - \mu_{\text{SS}}$ in lubricated condition.

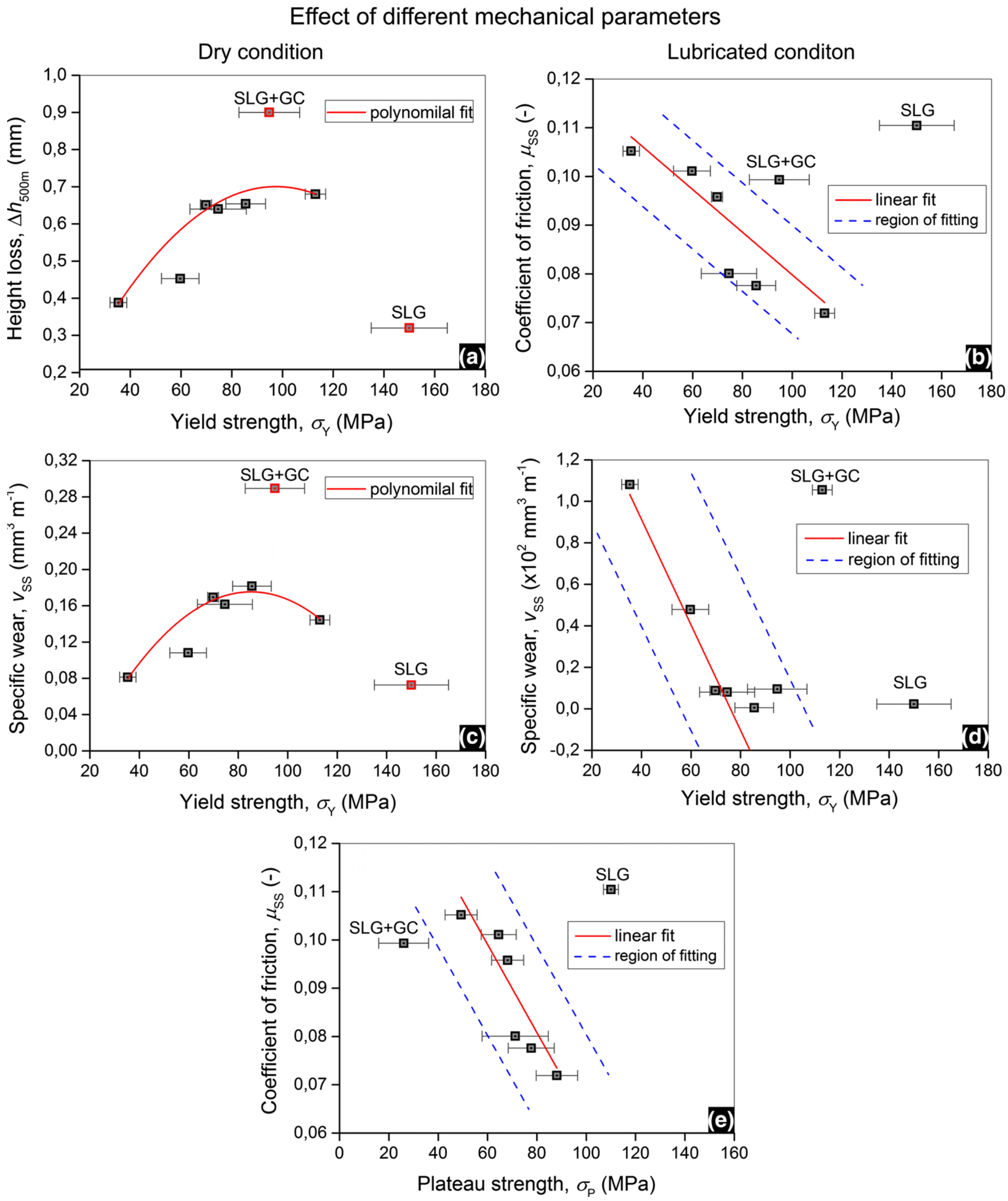

Figure 6. Correlation between; a) $\sigma_y - \Delta h_{500m}$, c) $\sigma_y - v_{SS}$ in dry condition and between; b) $\sigma_y - \mu_{SS}$, d) $\sigma_y - v_{SS}$, e) $\sigma_p - \mu_{SS}$ in lubricated condition.